Spatial Information Lasing Enabled by Full-k-space Bound States in the Continuum

Ruoheng Chai,[1] Wenwei Liu,[1,*] Zhancheng Li,[1] Yuebian Zhang,[1]
Haonan Wang,[1] Hua Cheng,[1,†] Jianguo Tian,[1] and Shuqi Chen[1,2,3,‡]

[1] *The Key Laboratory of Weak Light Nonlinear Photonics, Ministry of Education, School of Physics and TEDA Institute of Applied Physics, Nankai University, Tianjin 300071, China*
[2] *School of Materials Science and Engineering, Smart Sensing Interdisciplinary Science Center, Nankai University, Tianjin 300350, China*
[3] *The Collaborative Innovation Center of Extreme Optics, Shanxi University, Taiyuan 030006, China*

(Dated: March 31, 2024)

Optical amplification and massive information transfer in modern physics depend on stimulated radiation. However, regardless of traditional macroscopic lasers or emerging micro/nanolasers, the information modulations are generally outside the lasing cavities. On the other hand, bound states in the continuum (BICs) with inherently enormous Q factors are limited to zero-dimensional singularities in the momentum space. Here, we propose the concept of spatial information lasing, whose lasing information entropy can be correspondingly controlled by near-field Bragg coupling of guided modes. This concept is verified in gain-loss metamaterials supporting full-k-space BICs with both flexible manipulations and strong confinement of light fields. The counterintuitive high-dimensional BICs exist in a continuous energy band, which provide a versatile platform to precisely control each lasing Fourier component and thus can directly convey rich spatial information on the compact size. Single mode operation achieved in our scheme ensures consistent and stable lasing information. Our findings can be expanded to different wave systems and open new scenarios in informational coherent amplification and high-Q physical frameworks for both classical and quantum applications.

Laser technology can concentrate massive photons and load information thanks to its high spatiotemporal coherence, with profound impacts on both the research community and daily routines [1, 2]. Driven by the ultrasmall mode volume and lower power consumption, researchers have demonstrated various emerging laser systems, such as microcavity lasers [3], photonic bandgap lasers [4], nanolasers [5, 6], and topological lasers [7, 8]. Although there are various mode selection mechanisms [8–11], the state-of-the-art laser technology can hardly transfer rich spatial information without additional optical components [3–5, 7–17], such as interferometers and holograms, which limits optical interconnects and photonic integrations. According to Fourier optics, nonuniform wavefronts require multiple momentum components. However, additional in-plane momentums induced by finite boundaries [18] or supercells [16] inevitably lead to considerable mode competitions that are deleterious to coherent amplification.

On the other hand, recent advances in non-Hermitian photonics bring great opportunities to the micro/nanolaser systems. Non-Hermitian photonics describing ubiquitous open optical systems [19–22] has become a prominent research frontier because it creates intriguing physical concepts and applications, such as exceptional points (EPs) [21, 22], parity-time (PT) symmetry [22], unidirectional light propagation [23], and lasing/anti-lasing [24, 25]. Open systems are generally dissipative but can support real eigenvalues under PT symmetry. PT symmetry has been experimentally achieved by inducing loss difference or gain/loss to coupled cavity modes in various optical systems, such as metamaterials [26], microcavity [27], and waveguides [28]. The PT phase transition takes place at a singularity (i.e., EP) where both eigenvalues and eigenstates collapse [22]. Focusing on the radiating loss of non-Hermitian systems, bound states in the continuum (BICs) have been extensively explored since they provide extremely high Q factors at an ultrasmall scale [18, 29–34]. BICs refer to real spectra embedded in the radiation continuum by destructive interference induced by strong couplings [29]. However, BICs are recognized as zero-dimensional polarization singularities in the k-space [30, 31]. Yet the high-dimensional BIC in the momentum space has remained unexplored.

In this paper, inspired by non-Hermitian physics [26] and metamaterials locally tailoring optical responses [35–38], we propose the concept of informational lasing enabled by full-k BIC resonators that have infinite Q factors in a continuous energy band [Fig. 1(a)]. The intra-cavity lasing information entropy can be modified by changing the mode couplings, simultaneously maintaining the high-Q and net-gain properties. The lasing information entropy can be continuously tuned by an all-optical method or by configuring the complex Fourier components (CFCs) of the permittivity. Mode discrimination is achieved by exploiting the unidirectional scattering in the vicinity of EPs and the plane-wave seeding.

Distinct from conventional optical BICs whose Q factors decrease exponentially with deviation of k_{BICs}, the full-k BICs have infinite Q factors regardless of the wavevector [Fig. 1(b)]. To shed light on the full-k BICs, we begin with a two-level asymmetric non-Hermitian

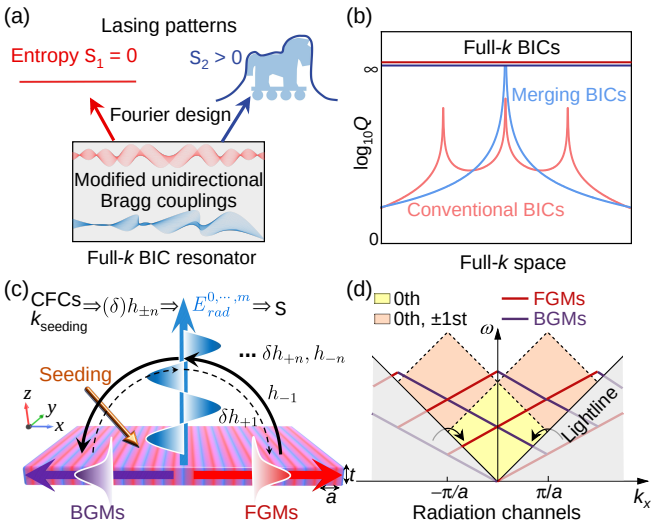

FIG. 1. (a) Schematic of spatial information lasing by a full-k BIC resonator. Lasing wavefronts and thus information can be engineered by modifying the lasing entropy inside the full-k BIC resonator. (b) Comparison between conventional k-sensitive BICs (light red line, conventional BICs; light blue line, merging BICs) and full-k-space BICs (deep red and deep blue lines). (c) Schematic of asymmetric couplings in the PTMMs. The CFCs combined with the momentum of seeding injection $k_{seeding}$ engineer the Bragg couplings $h_{\pm n}$, which determine the far-field Fourier components $E_{rad}^{0,\cdots,m}$, and thus the entropy $\mathcal{S}$. The thickness and the period of the PTMMs are t and $a = 2t$, respectively. (d) Simulated band diagram and radiation channel chart of uncoupled guided modes. The bands are folded above the light line by an assumed period a of a homogeneous slab with $\epsilon = 4$. Light yellow (pink) region, 0th-order (0th-, ±1st-order) diffraction channels; dark red (dark blue) lines, FGMs (BGMs).

Hamiltonian:

$$H = \begin{bmatrix} \omega & \delta\kappa_{\rightarrow} \\ \kappa_{\leftarrow} & \omega \end{bmatrix}, \tag{1}$$

where $\kappa_{\rightarrow}$ ($\kappa_{\leftarrow}$) represents forward (backward) couplings, and δ indicates that $\delta\kappa_{\rightarrow}$ is a perturbative small quantity.

To realize the asymmetric Hamiltonian, we consider a general PT-modulated metamaterial (PTMM), whose permittivity can be decomposed into a series of CFCs:

$$\mathcal{F}\left[\epsilon(x)\right] = \epsilon_0 + \sum_{n}^{+\infty} \delta\epsilon_{+n} e^{+ni(Kx+\phi_{+n})} + \epsilon_{-n} e^{-ni(Kx+\phi_{-n})}, \tag{2}$$

where n is a positive integer, ϵ_0 is the permittivity of a homogenous photonic slab, and $\epsilon_{\pm n}$ ($\phi_{\pm n}$) represents the amplitude (phase) of the $\pm n$th-order CFCs with in-plane momentum $\pm nK$ ($K = 2\pi/a$). $\delta\epsilon_{+n}$ is perturbatively small compared to ϵ_{-n}, which can be realized by gain-loss modulations. Note that the proposed modulation of CFCs is feasible [39]. The basis vectors of Eq. (1) can be chosen as two counter-propagating guided modes. Then the coupling terms [39] are expressed as:

$$\omega_{\pm}(k) = \omega(k) \pm \sqrt{\delta\kappa_{\rightarrow}\kappa_{\leftarrow}}, \tag{3a}$$

$$\kappa_{\leftrightarrow} = \sum_{i} \prod_{n,\nu} h^{\nu}(\epsilon_{\pm n}) \left[\left(\sum_{n,\nu} \pm n\nu \right) = \mathrm{sgn}(\leftrightarrow) N \right]_i, \tag{3b}$$

where $\omega(k)$ is the energy dispersion of uncoupled waveguide modes; $h^{\nu}(\epsilon_{\pm n})$ (hereinafter denoted as $h^{\nu}_{\pm n}$) are the coefficients representing the νth-order Bragg scattering processes by $\epsilon_{\pm n}$, which are proportional to the νth power of $\epsilon_{\pm n}$ and provide in-plane momentum $\pm n\nu K$; N is a positive integer denoting the dimensionless momentum difference between forward and backward guided modes (FGMs and BGMs) in the vicinity of the Nth stopband; $\mathrm{sgn}(\rightarrow) = +1$ and $\mathrm{sgn}(\leftarrow) = -1$ denote the coupling directions; the cumulative production represents successive Bragg processes; and the square brackets indicate all of the possible permutations of these Bragg processes that fulfil the conservation of in-plane momentum.

Equation (3b) suggests the coupling coefficients $\kappa_{\leftrightarrow}$ are expressed by multiple Bragg processes with multiple diffraction channels ($E_{rad}^{0,\cdots,m}$). For example, the forward (backward) couplings are $\kappa_{\leftarrow} = h^2_{-1}$ ($\delta\kappa_{\rightarrow} = \delta h^2_{+1}$), with 1st-order CFCs in the vicinity of the 2nd stopband ($N = 2$, the diffraction channels $m = 0$), as shown in Fig. 1(c). If the backward couplings $\delta\kappa_{\rightarrow}$ are removed by eliminating ϵ_{+1}, we obtain $\omega_{\pm}(k_x) = \omega(k_x)$, which means the PTMMs share the same bands with the uncoupled guided modes [Fig. 1(d)], manifesting Dirac dispersions, band degeneracies at high-symmetry k-points, and infinite Q factors regardless of the Bloch wavevectors (full-k BICs). In addition, the eigenstates solved from Eq. (1) coalesce into one BGM due to the extremely asymmetric couplings, forming EPs at high-symmetry k-points.

We start from a simplest form of PTMMs with 1st-order PT modulations:

$$\epsilon(x) = \epsilon_0 + \epsilon_1 \left[\cos(Kx) - iV_0 \sin(Kx)\right], \tag{4}$$

where V_0 denotes the imaginary to real part ratio of the modulation depth. It should be noticed that the specific optical constant profile can be discretized and realized by an index-contrast grating according to the effective medium theory, no necessity for a continuous control of CFCs [39]. We focus on TE-like modes as the principle of full-k BICs is independent of polarizations. The theoretical Q factors of the guided modes are diverging in the full k-space when $V_0 = 1$ [Fig. 2(a)]. The diverging Q factor is one of the signatures of ideal BICs, which means they are truly orthogonal to the radiative continuum. The simulated Q factors are divergent in the full-k space as well [39]. Note that the practical Q factor is always finite, limited by current nano-fabrication technology, e.g., fabrication error, surface roughness, material

intrinsic losses and finite array effects. The corresponding bands manifest perfect Dirac dispersions, as shown in Fig. 2(b). The degeneracy of both eigenvalues and eigenstates is demonstrated at high-symmetry k-points [inset graph of Fig. 2(b)], achieving coincidence between EPs and BICs.

Then we consider the Q factors of the PTMM in the two-dimensional momentum space (k_x, k_y), as shown in Fig. 2(c). The PTMM is firstly simplified as a cosine grating without gain-loss when $\arctan(1/|V_0|) = 90°$. In this case, band 1 manifests a typical at-Γ BIC and significantly reduced Q factors at off-Γ points. In contrast, the sinusoidal PTMM ($\arctan(1/|V_0|) = 45°$) shows infinite Q factors irrespective of the momentum, which is consistent with the C_2-symmetry-independent unidirectional couplings. The metamaterial is purely gain-loss modulated when $\arctan(1/|V_0|) = 0$, in which case, the corresponding mode becomes radiative modes. In short summary, the sinusoidal PTMM manifests BICs in the full (k_x, k_y) space and the balanced real/imaginary modulation is critical (system error analysis discussed in Ref. [39]).

The transition from BICs to quasi-BICs is crucial for building practical devices to realize efficient excitation [32]. We then discretize the sinusoidal PTMM as D-PTMM with the supercell composed of four euqal-size adjoining blocks: $\epsilon_0 + (1, -i, -1, i) \times \epsilon_{PT}$, where $\epsilon_{PT} = 0.4$ denotes the PT modulation depth. Such a CFC profile with resemble modulation depths and spatial gradient has been experimentally demonstrated [9, 23, 25, 28]. Compared with real-index modulated metamaterials [40, 41], the system is robust to the absolute gains and losses, but requires balancing between the two. The system tolerances of relative slab thickness and relative imbalance of real/imaginary modulation are approximately ±1% [39]. The permittivity can be expanded to the 3rd complex harmonics $\epsilon(x) = \epsilon_0 + \epsilon_{-1}e^{-iKx} + \epsilon_{+3}e^{+3iKx}$, and $\epsilon_{+3} = \epsilon_{-1}/3$ introduces perturbative back-couplings. Taking the X point with 0th- and 1st-order diffractions as an example, $\kappa_{\leftarrow} = h_{-1}^3$ and $\delta\kappa_{\rightarrow} = \delta h_{+3}$. For the D-PTMM, the Q factors can reach 10^3–$10^{4.5}$ and an avoided crossing are observed [Fig. 3(a)], achieving full-k quasi-BICs. The good agreement between theory and full-wave simulations suggests that the 3rd-order approximation is sufficient. The Q factors can be further improved based on the scaling-law of the quasi-BICs [39].

We then excited these quasi-BIC resonances in high-order diffraction regions by oblique plane-wave seeding injections with various in-plane momenta. The radiation energy spectra are demonstrated in Fig. 3(b), showing far-larger-than-unity total scattering energy. The scattering spectra imply that the radiation waves are coher-

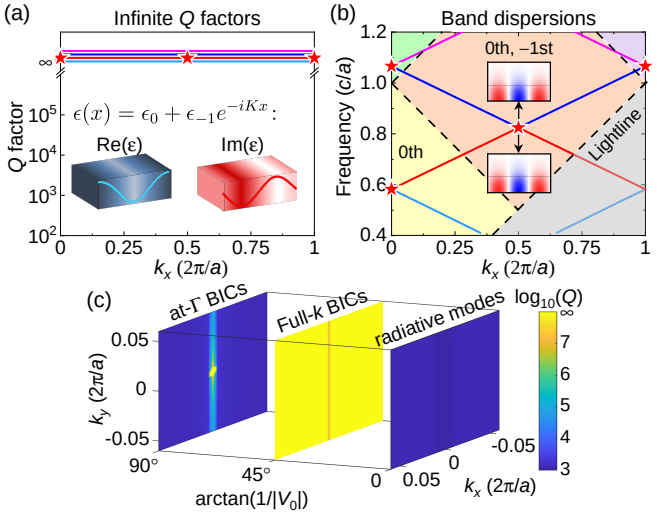

FIG. 2. (a) Theoretical Q factors and (b) simulated band dispersions of the sinusoidal PTMMs with the 1st-order CFC. The uniform term ϵ_0 is fixed at 4.0, the 1st-order term ϵ_1 is 0.4. Inset graphs show identical eigenstates at high-symmetry k-points, implying EPs. Colored regions represent different diffraction channels. Light blue, red, blue, magenta lines: band 1–4; red stars: EP-BIC coincidence points. (c) Simulated $Q(k_x, k_y)$ of band 1 versus $\arctan(1/|V_0|)$, where V_0 denotes the imaginary to real part ratio of the PT-modulation depth.

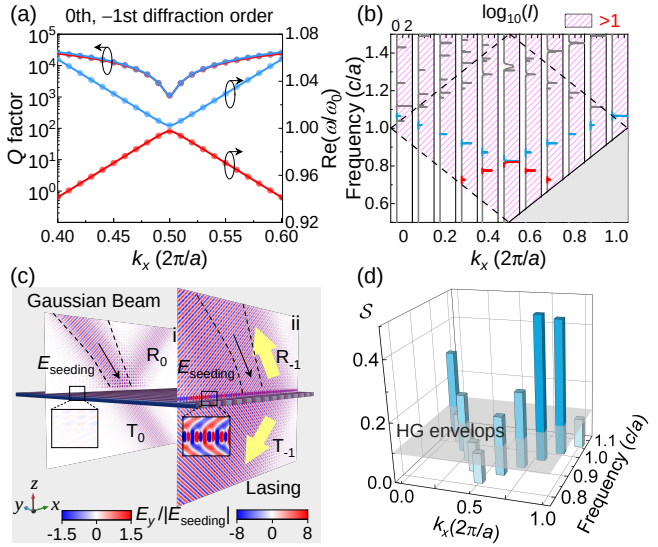

FIG. 3. (a) Bands and Q factors of full-k quasi-BICs supported by the D-PTMM (red, band 2; blue, band 3; dots, simulations; lines, theory). (b) Simulated spectrum of the total radiation energy I. The pink-hatched region highlights lasing zones. (c) Simulated mode profiles of band 3 at the X point at off-resonance (i) and on-resonance (ii) with a limited-spot Gaussian beam injection $E_{seeding}$ (waist radius $w_0 = 5\lambda_0$, where λ_0 is the incident wavelength). $R_{0,-1}$ ($T_{0,-1}$) are 0th and −1st order reflective (transmissive) lasing channels. (d) Calculated lasing information entropy $\mathcal{S}$ of band 3. Information entropy of Hermite-Gaussian envelopes (HG_0, HG_1, and HG_2) with cavity size $L = 100a$ is indicated by grey surfaces.

ently amplified at full-k quasi-BICs, leading to full-k lasing. The lasing action is attributed to more modal gain experience by the excited unidirectional BGMs (lossy FGMs not excited) in the spontaneously PT-broken phase that is determined by the balanced real and imaginary modulations. The full-k lasing (pink-hatched region) is not limited to the two bands in the vicinity of the 3rd stopband, but applicable to any other bands, such as the grey peaks and the additional peaks (high-order TE modes), which is consistent with the university of the unidirectional Bragg couplings. The strength of the Bragg scattering dramatically decreases when away from the band edge [42], which dominates over the effects of Q factors. Consequently, reduced lasing power is observed when away from the band edge.

The corresponding field distributions at X point are shown in Fig. 3(c). No near-field enhancement in the PTMM and regular reflection/transmission of Gaussian beams are observed at off-resonance [panel (i) in Fig. 3(c)]. In contrast, panel (ii) in Fig. 3(c) shows large-scale anomalous reflective/transmissive lasing with high directionality. The nonlocal travelling-wave features and net modal gain experienced by the full-k quasi-BICs give raise to the unidirectional propagation along the whole metamaterial even beyond the incident Gaussian beam spot [inset graph of (ii) in Fig. 3(c)]. Additionally, the discretized PT modulations induce energy leakage and in-plane momentum, leading to anomalous large-angle (X point, 36°) directional lasing, which can reach the theoretical limits (90°) when the bands approaching the light line.

To quantify the optical information induced by multiple orders of CFCs, we employ the famous Shannon's information entropy $\mathcal{S}$[43, 44]

$$\mathcal{S}(\nabla f) = -\sum_{i=i_{min}}^{i_{max}} p_i \log_N p_i, \tag{5}$$

which is defined based on the pixel gradient (pixel is defined as the Abbe diffraction limit) of the grey-scale image of the lasing far-field $\nabla f = \frac{\partial}{\partial x}|E_y|$, describing the nonuniformity of the lasing far-field [45]. $|E_y|(x)$ is the normalized absolute electric field. N is the bin-counts of ∇f. p_i is the probability of occurrence of the event $i = \nabla f$, where $\sum_{i=i_{min}}^{i_{max}} p_i = 1$, and $0 \le p_i \le 1$.

We then apply the information entropy $\mathcal{S}$ to the lasing fields of band 3 with various in-plane momentum seeding injections [Fig. 3(d)]. The lasing information entropy $\mathcal{S}$ can be tuned from approximately 0.1 to 0.45 by the incident angle of the seeding light. In contrast, the conventional lasing modes of Hermite-Gaussian (HG) envelops show low $\mathcal{S}$ of 0.1 since they are slow-varying. The greater complexity of the lasing patterns indicates an increased number of Fourier components (diffraction channels). This leads to the potential for achieving higher $\mathcal{S}$, reaching the maximum of 1, through the inclusion of more high-order diffractive lasing channels. Furthermore, the lasing information can be engineered on-demand via designing the amplitude and phase of each lasing Fourier component by configuring the CFCs of the PTMMs [39]. The high modulation bandwidth can be potentially achieved when involving dynamic modulations [46, 47], even with a slow modulation speed. This is mainly due to the introduction of a new dimension of spatial information in the process of laser generation.

The mode competition is critical in laser technology since it severely affects the beam qualities and lasing information. We discussed two types of mode competitions in this work: (1) Counter-propagating guided mode competitions in the vicinity of EPs, and (2) k-mode competitions, considering modes at general k-points can be selected by large free spectral range and gain dispersion. We can obtain the steady-state bifurcation diagrams by laser rate equations (Fig. 4). As shown in Fig. 4(a), the BGM mode dominates over the FGM mode as a result of the asymmetric Bragg couplings ($\kappa_{\rightarrow}/\kappa_{\leftarrow} = 0$) in the vicinity of EPs. Single-k-mode lasing of mode k1 is achieved and mode k2 is fully suppressed at completely asymmetric external coupling condition ($\kappa_{ext2}/\kappa_{ext1} = 0$), as shown in Fig. 4(b) [48]. This is intuitive since mode k1 starts lasing from seeding photons while mode k2 from quantum noise. The single-mode (k-mode) lasing is robust against the asymmetric mode (external) coupling factor $\kappa_{\rightarrow}/\kappa_{\leftarrow}$ ($\kappa_{ext2}/\kappa_{ext1}$) [39].

Interestingly, the directionality can be engineered from almost zero diverging angle [plane-wave wavefront in single channel lasing, Fig. 3(c)] to wide-angle multidirectional lasing by tuning the incident angle of the seeding injection or configuring the CFCs. The reconfigurable directionality of the PTMMs outperforms the traditional nanolasers. The continuous-wave and pulsed operations are compatible within our scheme thanks to the single-mode (k-mode) operation avoiding multimode interactions such as mode locking and alternate oscillations.

There are two crucial characteristics for the informational lasing based on full-k BICs. One is the high-Q and

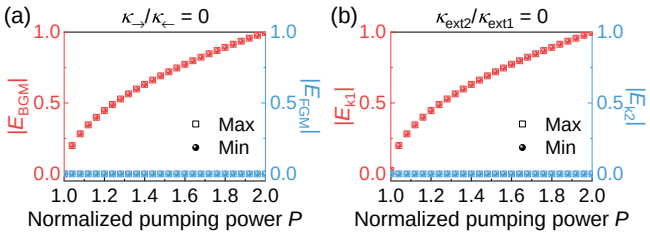

FIG. 4. Bifurcation diagrams calculated by the laser rate equations, depicting the steady-state maximum and minimum of the amplitude $|E(t)|$ versus the normalized pumping power P ($P = 1$ at the threshold) in the case of (a) band mode competitions, and (b) k-mode competitions. $\kappa_{\rightarrow}/\kappa_{\leftarrow}$ ($\kappa_{ext2}/\kappa_{ext1}$) is the asymmetric mode (external) coupling factor in the rate equations.

full-k-space trapping of photons lying above the light line, which is fundamentally very hard to achieve in conventional laser cavities, if at all. Another point concerns single-mode (k-mode) lasing operation with information modulations inside the laser cavity. The intensity and phase in each information channel is strictly constrained by the momentum-conservative Bragg scatterings. This type of spatial information modulation exploits nonlocal states with adaptable Bragg couplings, which is challenging for conventional nanolasers with a localized-state signature [6].

In conclusion, we proposed an asymmetric-coupled system for intra-cavity informational lasing enabled by full-k BICs. As a proof of concept, we designed PTMMs to demonstrate spatial informational lasing engineered by an all-optical method or CFC configurations. Single mode operation can be achieved by exploiting the unidirectional Bragg couplings and the seeding injection. Serving as both light sources and information modulators with enhanced light-matter interactions, spatial information lasing of full-k BICs opens new horizons for highly-integrated information amplification, which will promote the progress of nonlinear physics, photonic integrated circuits, and on-chip quantum computing.

This work was supported by the National Key Research and Development Program of China (2021YFA1400601 and 2022YFA1404501), the National Natural Science Fund for Distinguished Young Scholar (11925403), and the National Natural Science Foundation of China (12122406, 12192253, 12274239, and U22A20258).

* Corresponding author: wliu@nankai.edu.cn
† Corresponding author: hcheng@nankai.edu.cn
‡ Corresponding author: schen@nankai.edu.cn

[1] W. T. Silfvast, *Laser fundamentals*, 2nd ed. (Cambridge University Press, Cambridge, 2004).
[2] R. Slusher, Rev. Mod. Phys. **71**, S471 (1999).
[3] X. Qiao, B. Midya, Z. Gao, Z. Zhang, H. Zhao, T. Wu, J. Yim, R. Agarwal, N. M. Litchinitser, and L. Feng, Science **372**, 403 (2021).
[4] O. Painter, R. K. Lee, A. Scherer, A. Yariv, J. D. O'Brien, P. D. Dapkus, and I. Kim, Science **284**, 1819 (1999).
[5] R.-M. Ma and R. F. Oulton, Nat. Nanotechnol. **14**, 12 (2019).
[6] X.-R. Mao, Z.-K. Shao, H.-Y. Luan, S.-L. Wang, and R.-M. Ma, Nat. Nanotechnol. **16**, 1099 (2021).
[7] R. Contractor, W. Noh, W. Redjem, W. Qarony, E. Martin, S. Dhuey, A. Schwartzberg, and B. Kanté, Nature **608**, 692 (2022).
[8] L. Yang, G. Li, X. Gao, and L. Lu, Nat. Photonics **16**, 279 (2022).
[9] L. Feng, Z. J. Wong, R.-M. Ma, Y. Wang, and X. Zhang, Science **346**, 972 (2014).
[10] M. P. Hokmabadi, N. S. Nye, R. El-Ganainy, D. N. Christodoulides, and M. Khajavikhan, Science **363**, 623 (2019).
[11] R. Morita, T. Inoue, M. D. Zoysa, K. Ishizaki, and S. Noda, Nat. Photonics **15**, 311 (2021).
[12] Y.-Y. Xie, P.-N. Ni, Q.-H. Wang, Q. Kan, G. Briere, P.-P. Chen, Z.-Z. Zhao, A. Delga, H.-R. Ren, H.-D. Chen, *et al.*, Nat. Nanotechnol. **15**, 125 (2020).
[13] C. Huang, C. Zhang, S. Xiao, Y. Wang, Y. Fan, Y. Liu, N. Zhang, G. Qu, H. Ji, J. Han, *et al.*, Science **367**, 1018 (2020).
[14] Z.-Q. Yang, Z.-K. Shao, H.-Z. Chen, X.-R. Mao, and R.-M. Ma, Phy. Rev. Lett. **125**, 013903 (2020).
[15] Y. Yu, A. Sakanas, A. R. Zali, E. Semenova, K. Yvind, and J. Mørk, Nat. Photonics **15**, 758 (2021).
[16] C. Spägele, M. Tamagnone, D. Kazakov, M. Ossiander, M. Piccardo, and F. Capasso, Nat. Commun. **12**, 3787 (2021).
[17] X. Zhang, Y. Liu, J. Han, Y. Kivshar, and Q. Song, Science **377**, 1215 (2022).
[18] A. Kodigala, T. Lepetit, Q. Gu, B. Bahari, Y. Fainman, and B. Kanté, Nature **541**, 196 (2017).
[19] R. El-Ganainy, K. G. Makris, M. Khajavikhan, Z. H. Musslimani, S. Rotter, and D. N. Christodoulides, Nat. Phys. **14**, 11 (2018).
[20] L. Feng, R. El-Ganainy, and L. Ge, Nat. Photonics **11**, 752 (2017).
[21] M.-A. Miri and A. Alù, Science **363**, eaar7709 (2019).
[22] Ş. K. Özdemir, S. Rotter, F. Nori, and L. Yang, Nat. Mater. **18**, 783 (2019).
[23] L. Feng, Y.-L. Xu, W. S. Fegadolli, M.-H. Lu, J. E. B. Oliveira, V. R. Almeida, and A. Chen, Yan-Feng Scherer, Nat. Mater. **12**, 108 (2013).
[24] Y. D. Chong, L. Ge, and A. D. Stone, Phys. Rev. Lett. **106**, 093902 (2011).
[25] Z. J. Wong, Y.-L. Xu, J. Kim, Y. O'Brien, Kevin Wang, L. Feng, and X. Zhang, Nat. Photonics **10**, 796 (2016).
[26] X. Yin and X. Zhang, Nat. Mater. **12**, 175 (2013).
[27] H. Hodaei, M.-A. Miri, M. Heinrich, D. N. Christodoulides, and M. Khajavikhan, Science **346**, 975 (2014).
[28] P. Miao, Z. Zhang, J. Sun, W. Walasik, S. Longhi, N. M. Litchinitser, and L. Feng, Science **353**, 464 (2016).
[29] C. W. Hsu, B. Zhen, A. D. Stone, J. D. Joannopoulos, and M. Soljačić, Nat. Rev. Mater. **1**, 16048 (2016).
[30] B. Zhen, C. W. Hsu, L. Lu, A. D. Stone, and M. Soljačić, Phys. Rev. Lett. **113**, 257401 (2014).
[31] J. Jin, X. Yin, L. Ni, M. Soljačić, B. Zhen, and C. Peng, Nature **574**, 501 (2019).
[32] K. Koshelev, S. Lepeshov, M. Liu, A. Bogdanov, and Y. Kivshar, Phys. Rev. Lett. **121**, 193903 (2018).
[33] B. Wang, W. Liu, M. Zhao, J. Wang, Y. Zhang, A. Chen, F. Guan, X. Liu, L. Shi, and J. Zi, Nat. Photonics **14**, 623 (2020).
[34] R. Chai, W. Liu, Z. Li, H. Cheng, J. Tian, and S. Chen, Phys. Rev. B **104**, 075149 (2021).
[35] J. B. Pendry, Phys. Rev. Lett. **85**, 3966 (2000).
[36] R. A. Shelby, D. R. Smith, and S. Schultz, Science **292**, 77 (2001).
[37] J. Yao, Z. Liu, Y. Liu, Y. Wang, C. Sun, G. Bartal, A. M. Stacy, and X. Zhang, Science **321**, 930 (2008).
[38] S. Chen, W. Liu, Z. Li, H. Cheng, and J. Tian, Adv. Mater. **32**, 1805912 (2020).
[39] See Supplemental Material at http://xxxx.xxx.xxx for

the detailed derivation of formulas and discussions: dispersion relations of the 1st-order sinusoidal PTMMs; dispersion relations of the D-PTMM; Q factors diverging to infinity; manipulations of the absolute diffraction lasing amplitudes; comprehensive spatial information lasing by configuring CFCs of permittivity; mode (k-mode) competition analysis; feasible protocols and error analysis, which includes Refs. [49–66].

[40] K. L. Tsakmakidis, A. D. Boardman, and O. Hess, Nature **455**, E11 (2008).

[41] K. L. Tsakmakidis, O. Hess, R. W. Boyd, and X. Zhang, Science **358**, eaan5196 (2017).

[42] K. Inoue and K. Ohtaka, *Photonic Crystals: Physics, Fabrication and Applications* (Springer-Verlag, New York, 2004).

[43] R. M. Haralick, K. Shanmugam, and I. Dinstein, IEEE Trans. Syst. Man Cybern. **SMC-3**, 610 (1973).

[44] J. C. Russ, *The Image Processing Handbook*, 6th ed. (CRC press, 2011).

[45] Note that $\mathcal{S}$ is normalized from 0 to 1, and is distinctive from the thermal dynamic entropy. $\mathcal{S}$ is defined spatially, reflecting the capacity of the spatial information channels (Fourier components) of the lasing far-field. The information entropy $\mathcal{S}$ can be directly measured by detecting the far-field intensity distribution f using optoelectronic devices and optical imaging system, which is same as the measurement of holography.

[46] F. Gardes, K. Tsakmakidis, D. Thomson, G. Reed, G. Mashanovich, O. Hess, and D. Avitabile, Opt. Express **15**, 5879 (2007).

[47] Z. Lin, Y. Lin, H. Li, M. Xu, M. He, W. Ke, H. Tan, Y. Han, Z. Li, D. Wang, *et al.*, Light Sci. Appl. **11**, 93 (2022).

[48] The k-mode selection is achieved by an external seeding injection with specific in-plane momentum k_1 and frequency ω_1. The k modes have asymmetric external couplings with the seeding injection due to the different momentum and frequency overlapping between k modes and seeding injection.

[49] S.-G. Lee, S.-H. Kim, and C.-S. Kee, Phys. Rev. Lett. **126**, 013601 (2021).

[50] Y. Liang, K. Koshelev, F. Zhang, H. Lin, S. Lin, J. Wu, B. Jia, and Y. Kivshar, Nano Lett. **20**, 6351 (2020).

[51] K. Koshelev, S. Lepeshov, M. Liu, A. Bogdanov, and Y. Kivshar, Phys. Rev. Lett. **121**, 193903 (2018).

[52] M. Sorel, P. Laybourn, A. Scirè, S. Balle, G. Giuliani, R. Miglierina, and S. Donati, Opt. Lett. **27**, 1992 (2002).

[53] M. Sorel, G. Giuliani, A. Scire, R. Miglierina, S. Donati, and P. Laybourn, IEEE J. Quantum. Electron. **39**, 1187 (2003).

[54] I. Stamataki, S. Mikroulis, A. Kapsalis, and D. Syvridis, IEEE J. Quantum. Electron. **42**, 1266 (2006).

[55] X. Cai, Y.-L. D. Ho, G. Mezosi, Z. Wang, M. Sorel, and S. Yu, IEEE J. Quantum. Electron. **48**, 406 (2012).

[56] T.-P. Lee, C. Burrus, J. Copeland, A. Dentai, and D. Marcuse, IEEE J. Quantum. Electron. **18**, 1101 (1982).

[57] T. Yee and D. Welford, IEEE J. Quantum. Electron. **22**, 2116 (1986).

[58] M. Schell, W. Utz, D. Huhse, J. Kässner, and D. Bimberg, Appl. Phys. Lett. **65**, 3045 (1994).

[59] G. Yuan and S. Yu, IEEE J. Quantum. Electron. **44**, 41 (2007).

[60] W. Wang, L.-Q. Wang, R.-D. Xue, H.-L. Chen, R.-P. Guo, Y. Liu, and J. Chen, Phys. Rev. Lett. **119**, 077401 (2017).

[61] Q. Song, J. Hu, S. Dai, C. Zheng, D. Han, J. Zi, Z. Q. Zhang, and C. T. Chan, Sci. Adv. **6**, eabc1160 (2020).

[62] Y. Xu, L. Li, H. Jeong, S. Kim, I. Kim, J. Rho, and Y. Liu, Sci. Adv. **9**, eadf3510 (2023).

[63] R. Yao, C.-S. Lee, V. Podolskiy, and W. Guo, Laser Photonics Rev. **13**, 1800154 (2019).

[64] K.-H. Kim, M.-S. Hwang, H.-R. Kim, J.-H. Choi, Y.-S. No, and H.-G. Park, Nat. Commun. **7**, 13893 (2016).

[65] L. Feng, M. Ayache, J. Huang, Y.-L. Xu, M.-H. Lu, Y.-F. Chen, Y. Fainman, and A. Scherer, Science **333**, 729 (2011).

[66] M. P. Hokmabadi, N. S. Nye, R. El-Ganainy, D. N. Christodoulides, and M. Khajavikhan, Science **363**, 623 (2019).